



Published in final edited form as:

Orthod Craniofac Res. 2015 April ; 18(0 1): 18–28. doi:10.1111/ocr.12070.

3D superimposition and understanding temporomandibular joint arthritis

LHS Cevidanes^a, LR Gomes^{a,b}, BT Jung^c, MR Gomes^d, ACO Ruellas^{a,e}, JR Goncalves^b, J Schilling^f, M Styner^g, T Nguyen^c, S Kapila^a, and B Paniagua^g

^aDepartment of Orthodontics and Pediatric Dentistry, University of Michigan, Ann Arbor, MI, USA

^bDepartment of Orthodontics and Pediatric Dentistry, Universidade Estadual Paulista, Araraquara, Sao Paulo, Brazil

^cDepartment of Orthodontics, University of North Carolina, Chapel Hill, NC, USA

^dPrivate Practice, Salvador, BA, Brazil

^eDepartment of Orthodontics, Federal University of Rio de Janeiro, Rio de Janeiro, Brazil.

^fDepartment of Periodontics and Oral Medicine, University of Michigan, Ann Arbor, MI, USA

^gDepartment of Psychiatry, University of North Carolina, Chapel Hill, NC, USA

Abstract

Objectives—To investigate the 3D morphological variations in 169 Temporomandibular Joint (TMJ) condyles, using novel imaging statistical modeling approaches.

Setting and Sample Population—The Department of Orthodontics and Pediatric Dentistry at the University of Michigan. Cone beam CT scans were acquired from 69 subjects with long-term TMJ osteoarthritis (OA, mean age 39.1 ± 15.7 years), 15 subjects at initial consult diagnosis of OA (mean age 44.9 ± 14.8 years) and 7 healthy controls (mean age 43 ± 12.4 years).

Material & Methods—3D surface models of the condyles were constructed and homologous correspondent points on each model were established. The statistical framework included Direction-Projection-Permutation (DiProPerm) for testing statistical significance of the differences between healthy controls and the OA groups determined by clinical and radiographic diagnoses.

Results—Condylar morphology in OA and healthy subjects varied widely with categorization from mild to severe bone degeneration or overgrowth. DiProPerm statistics supported a significant difference between the healthy control group and the initial diagnosis of OA group ($t=6.6$, empirical p -value = 0.006), and between healthy and long term-diagnosis of OA group ($t = 7.2$, empirical p -value = 0). Compared with healthy controls, the average condyle in OA subjects was significantly smaller in all dimensions, except its anterior surface, even in subjects with initial diagnosis of OA.

Correspondence: Lucia Cevidanes, Department of Orthodontics and Pediatric Dentistry, University of Michigan 1011 North University Avenue Ann Arbor, Michigan, 48109 1919 3578603, luciacev@umich.edu.

Conflict of interest statement:

This is an original work that has not been, submitted for publication or presentation elsewhere. All authors had no financial and personal relationships with other people or organizations that could inappropriately influence (bias) their work.

Conclusion—This new statistical modeling of condylar morphology allows the development of more targeted classifications of this condition than previously possible.

Keywords

TMJ condyle; bone degeneration; bone overgrowth

Introduction

When the temporomandibular joint (TMJ) presents with initial signs of destruction and inflammation, it is essential to monitor active disease, either localized to the TMJ or systemic, before loading the joints with orthodontic/orthopedic forces or undertaking jaw surgery.

The TMJ differs from other joints because a layer of fibrocartilage, and not hyaline cartilage, covers it (1). The bone of the mandibular condyles is located just beneath the fibrocartilage, making it particularly vulnerable to inflammatory damage and a valuable model for studying arthritic bony changes. The condylar bone is the site of numerous dynamic morphological transformations, which are an integral part of the initiation/progression of arthritis, not merely secondary manifestations to cartilage degradation. Thus, a strong rationale exists for therapeutic approaches that target bone resorption and formation (2-7).

The Research Diagnostic Criteria for temporomandibular disorders validation project (8,9) concluded that clinical criteria alone, without the use of imaging, are inadequate for valid diagnosis of TMJ arthritis. The application of cone beam CT (CBCT) to craniofacial imaging, with an adequate acquisition protocol, provides a clear visualization of the hard tissues of the TMJ and markedly reduces radiation and cost compared to medical CT (10) (Figure 1).

Methods for the registration of 3D condylar morphology are essential for the measurement of subtle bony differences in condylar morphology. The regional superimposition techniques, used in the present study for across subject comparisons, have been validated by Schilling et al. (11). The objective of the current study is to determine 3D morphological variations in asymptomatic controls, subjects at initial TMJ OA diagnosis and subjects with long-term history of TMJ OA, using 1002 imaging biomarkers. The working hypothesis is that bone morphology is characteristically different in OA compared to controls even at early diagnosis.

Methods

Sixty nine subjects with long-term TMJ OA (mean age 39.1 ± 15.7 years), 15 subjects at initial consult diagnosis of TMJ OA (mean age 44.9 ± 14.8 years) and 7 healthy controls (mean age 43 ± 12.4 years), recruited from the university clinic and through advertisement, underwent a clinical exam by an orofacial pain specialist. For the initial diagnosis group, only subjects with recent histories of pain, within the last 2 months, were included. For the long-term diagnosis, 13 subjects had only one condyle included as the other side joint had

prior history of interventions (joint injections, arthrocentesis or other pathologies, such as ankylosis (Figure 2). Recruitment and clinical exam diagnoses of TMJ osteoarthritis or health were confirmed by CBCT images (8, 9). The imaging protocol consisted of a 20-second scan, using a large field of view to include both TMJs and the same machine (i-Cat@ CBCT, 120 kV, 18.66 mA, Imaging Sciences, Hatfield, PA). The university institutional review board approved this study and all subjects were consented.

Image analysis methods

The flow chart in Figure 3 describes an overview of the image analysis procedures introduced by Schilling et al (11). All scan volumes were sliced to a voxel size of 0.5 mm³ (Figure 3B) to standardize voxel size, decrease the computational power and time required to compute the automated registration, using open-source software (3D Slicer v. 4.3.1, (<http://www.slicer.org>) (12).

3D surface mesh models of the right and left mandibular condyles were constructed by semi-automatic discrimination procedures that outlined the cortical boundaries of the condylar region and allowed manual editing, checking slice by slice in all three planes of space (Figure 3C) using open-source software (ITK-SNAP software v.2.4., www.itksnap.org) (13). After generating all 3D surface models, left condyles were mirrored in the sagittal plane to form right condyles to facilitate comparisons (Figure 3D).

Owing to individual morphological variability across subjects, voxel-based approaches fail, and a landmark-based approach was used to approximate consistently all condyles in the same coordinate system (11). The surface mesh files for each condyle were opened in surface analysis software (VAM v. 3.7.6, Canfield 113 Scientific Inc., Fairfield, NJ), and 25 landmarks were placed on each condylar surface model: 4 points evenly spaced along the superior surface of the sigmoid notch, 4 on the medial and 4 on the lateral portions of the ramus adjacent to the sigmoid notch, 3 along the posterior surface of the neck, 3 on medial and 3 on lateral portions of the neck, and 1 on the medial, 1 lateral, 1 anterior, and 1 posterior extremes of the condylar head (Figure 3E, 4A). The 25 landmarks were used only for spatial approximation of all condyles in a common arbitrary xyz co-ordinate system (Figure 4B). That is, the 25 landmarks were used only for registration of all surface models and not for analysis of morphological variability. After registration, all 3D surface models were simultaneously clipped/cropped to define the condylar region of interest and open-source software (SPHARM-PDM software, <http://www.nitrc.org/projects/spharm-pdm>) (14-17) was used to generate a mesh approximation from the volumes, whose points were mapped to a “spherical map” (Figure 3F). The homology/correspondence of the mapping of the 1002 points across all subjects (Figure 4C) was verified with color-coded maps of the surface parameterization (Figure 3G).

Creation of the average mesh—An average 3D condylar shape was generated for the two TMJ OA groups and control group (Figures 3H, 4A, 5A). The core of the ability to compute the group average and group variability is the establishment of correspondence (homology) between each of the 1002 points in the condylar surface models across all subjects. This allows the association of any of the 1002 points’ locations on the condyle of

subject A with the corresponding locations on the condyle of subject B, C... n number of subjects. Considerable intersubject variability is also accounted for in the model that captures the average condylar morphology and variability around that average morphology. Open-source software (Linux MeshMath script, <http://www.nitrc.org/projects/spharm-pdm>) (17) was used to create average meshes for the control, initial diagnosis and long-term history of OA groups. The 3D morphological variability of the 1002 surface point correspondences was used for surface mesh averaging. The affine transformations of the 3D morphological variability were then applied to the 1002 points on the condylar surface individually. In geometry, an affine transformation is a transformation which preserves ratios of distances between points lying on a surface model, where parallel lines will remain parallel to each other after an affine transformation. Grouping all the mean points provided the linear and nonlinear deformation fields that resulted in the average condyle shape for each group.

Calculation of absolute and signed distances and vector differences—The MeshMath script was then used to calculate 3D point-wise subtractions between each group's average morphology (Figure 3Ia, 3Ib). The computed 1002 vector differences were displayed on the condyle surface, scaled according to the magnitude of difference and pointing in the direction of change. The patterns of variation across TMJ OA and control samples were determined through calculation of signed distances, where the areas of bone resorption were displayed as negative values (blue), no differences (0 mm surface distances, white) or bone proliferation as positive (red).

Control of the quality of the signed distances—Semi-transparent overlays between the average models in 3D Slicer software were used to compare visually the signed distance patterns.¹⁴

Statistical analysis—The statistical framework for testing condylar morphological variations included a Hotelling T-squared test in a multivariate analysis of covariance open-source software (Shape Analysis MANCOVA, Figure 3Ic) (18-19) corrected for false discovery rate at 0.05. For testing a high dimensional hypothesis, Direction-Projection-Permutation (DiProPerm) (20), rigorously tested lower dimensional graphical visual differences: direction (projected samples onto an appropriate direction), projection (calculated univariate two sample statistics) and permutation (assessed significance using 1000 permutations of group membership). The approach of Distance Weighted Discrimination (DWD) calculated a direction vector to classify high dimensional datasets, and their principal components (PC) were graphically plotted. The vector space is a mathematical structure formed by the collection of surface vectors that is called the feature space. Because the control and OA samples had different sample sizes, an appropriately weighted version of DWD, wDWD, was used to find a direction vector in the feature space separating the diagnostic groups.

Results

The semi-transparent overlays revealed that compared to healthy controls, the initial TMJ OA diagnosis group showed marked condylar bone changes and that these bone changes

were even more marked in the long-term TMJ OA group (Figure 5A, 5B). The mean OA models were of smaller size in all dimensions and areas of statistically significant differences were in the superior articular surface of the condyles, particularly in the anterior and superior portion of the lateral pole. That is, average bone resorption in this area was -2.7 mm in the initial TMJ OA diagnosis group and -4.2 mm in the long-term TMJ OA group as compared to the healthy control group (Figure 5C). In the anterior surface of the condyle, on average, a small area of 1.2mm of bone apposition was noted in the initial TMJ OA diagnosis group and of 3.5mm in the long-term TMJ OA group compared to the healthy control group (Figure 5C). When the initial diagnosis and long term OA average condylar models were compared, statistically significant differences indicative of more bone resorption in the long-term OA group were noted along the whole condylar surface except at the superior surface of the lateral pole. Subgroups were established by comparison of each individual condyle and the healthy controls' average condylar morphology (Figure 6).

The DiProPerm test found statistically significant morphological differences between the healthy control and the OA groups (Figure 7A; p-value = 0.001), between the healthy controls and the initial OA group (Figure 7B; p-value = 0.006), between the initial diagnosis and long-term diagnosis of OA groups (Figure 7C; p-value = 0.0009) and between the healthy controls and the long-term diagnosis of OA groups (Figure 7D: p-value = 0). The projection plots of healthy control condyles (red circles in Figure 7A) tend to cluster and are clearly separated from the OA groups. Most projected plots of initial OA diagnosis condyles are located within the bounds of the plots of the long-term OA diagnosis condyles (Figure 7A, 7B, 7C). The maximal partition of condylar morphology, as established by 1002 points in each individual condyle, can be observed in the graphic plots of the principal component refined in the wDWD direction. The wDWD direction onto the PC was shown by the angle in the PC analysis score plots shown in Figure 7D. Figure 8, in the manuscript online version, shows that while individual morphology variability occurs in the OA patients, the principal component of deformation markedly reveals the flattening of the lateral pole (sequence of images as the .gif file animation plays).

Discussion

These study findings revealed imaging biomarkers of the bone morphology differences at the articular surfaces of the condyle that can now be quantitatively tested by statistical imaging methods. The novel aspect of this study is that, even though the ability to predict progression was not addressable in the cross-sectional study design, these biomarkers can be reasonable surrogate biomarkers of tissue destruction and/or repair overtime.

The methods used in this study included open source image analysis software. Commercial software packages produce adequate surface reconstructions and/or offer landmark, surface and/or voxel-based registration methods, but they are not open source, cannot be modified, do not interact well with each other, do not provide flexibility for customization and, moreover, do not address the 3D correspondence problem across subjects with different facial morphology or from pre- and post-surgery scans of the same patient. Due to its open licensing, 3D Slicer has allowed specific implementation of modules for assessment of condylar changes and their detailed tutorials are now available (e.g. at www.youtube.com/

channel/UCQUtGe5KrpBt2k4mrNeHeUQ). 3D Slicer version 4 provides powerful tools for multimodal imaging, volume rendering, registration and visualization.

Due to great individual morphological variability across subjects, rigid-voxel-based approaches fail to register anatomic structures from different subjects in populational or group average studies. Other voxel-based registration approaches, that are fluid or semi-fluid (21), lead to changes and deformation of the morphology of the surface models, known as morphing, and the morphing hampers adequate evaluation of individual morphology. For these reasons, the registration across subjects in this study used an initial landmark-based approach to approximate all condyles in a common arbitrary xyz co-ordinate system (as shown in Figure 4). This initial procedure only aimed to approximate all condyles and allow the automatic computation of 1002 correspondent surface points for all condyles in a consistent way.

Our findings-C, that most plot projections of initial OA diagnosis condyles were located within the bounds of the long-term diagnosis condyles (Figure 7A), may be explained by the fact that both groups present characteristic osteoarthritic changes. The characteristic osteoarthritic changes observed in this study consisted of flattening of the lateral pole and bony projections in the anterior condylar surface, at initial diagnosis and significantly more marked at long-term diagnosis. It is possible that, even though the initial OA diagnosis group included only subjects with histories of pain within the last 2 months, the condition could have been of long-standing but asymptomatic for the individual. Interestingly, some of the plots of the condyles at initial diagnosis were projected toward the healthy control group. This may be explained by the fact that in patients with diagnosis of OA, the disease progression usually affects one joint first, while morphological changes may be less evident in the contralateral TMJ, particularly at initial diagnosis.

The present study findings represent a preliminary step toward an index of osteoarthritic changes. Our research group's long term goals are to implement statistical measurements that allow early detection of the degree of bone destruction and/or bone proliferation in any individual joint (22-23). Such an early diagnosis index is beyond the scope of the present work and will require larger control and OA samples, longitudinal studies and further statistical description of combinatorial biomarker assessments, such as receiver operating characteristic (ROC) curves on disease versus health, as well as classification-based schemes for computer-aided diagnosis of TMJ OA.

Importantly, an emerging theme in OA is a broadening of focus from a disease of cartilage to a disease of the entire joint and the multiple biological systems that interact with one another in this disease.(24) The cross-talk that occurs between the components of the joint, which takes place over years, results in degradation of the articular cartilage and disc, bony changes, synovial proliferation, muscle and tendon weakness, and fatigue. The condyle is the site of numerous dynamic morphologic transformations in the initiation/progression of OA,(25-28) which are not merely manifestations secondary to cartilage degradation. Thus, a strong rationale exists for therapeutic approaches that target bone resorption and formation and take into account the complex cross-talk between all of the joint tissues. While this study focused on bone morphological variability, greater understanding of mechanisms in

this multi-tissue disease requires a combination of imaging technologies, using methods that facilitate superimposition of soft and hard tissue data sets.

Conclusions

This new statistical modeling of condylar morphology allows the development of more targeted statistical classifications of TMJ OA than previously possible. Compared with healthy controls, the average condyle in OA subjects was significantly smaller in all dimensions, except its anterior surface, even in subjects with initial diagnosis of OA.

Acknowledgements

This work was supported by the National Institute Of Dental & Craniofacial Research of the National Institutes of Health under Award Number R01DE024450. The content is solely the responsibility of the authors and does not necessarily represent the official views of the National Institutes of Health

References

1. Wadhwa S, Kapila S. TMJ disorders: Future innovations in diagnostics and therapeutics. *Journal of Dental Education*. 2008; 72:930–947. [PubMed: 18676802]
2. Hayami T, Pickarski M, Wesolowski GA, McLane J, Bone A, Destefano J, et al. The role of subchondral bone remodeling in osteoarthritis: reduction of cartilage degeneration and prevention of osteophyte formation by alendronate in the rat anterior cruciate ligament transection model. *Arthritis Rheum*. 2004; 50:1193–206. [PubMed: 15077302]
4. Abramson SB, Attur M. Developments in the scientific understanding of osteoarthritis. *Arthritis Res Ther*. 2009; 11:227. [PubMed: 19519925]
5. Karsdal MA, Martin TJ, Bollerslev J, Christiansen C, Henriksen K. Are nonresorbing osteoclasts sources of bone anabolic activity? *J Bone Miner Res*. 2007; 22:487–494. [PubMed: 17227224]
6. Hunter DJ, Eckstein F, Kraus VB, Losina E, Sandel L, Guermazi A. Imaging Biomarker Validation and Qualification Report: Sixth OARSI Workshop on Imaging in Osteoarthritis combined with Third OA. Biomarkers Workshop. *Osteoarthritis and Cartilage*. 2013; 21:939–942. [PubMed: 23639411]
7. Bauer DC, Hunter DJ, Abramson SB, Attur M, Corr M, Felson D, et al. Classification of osteoarthritis biomarkers: A proposed approach. *Osteoarthritis and Cartilage*. 2006; 14:723–727. [PubMed: 16733093]
8. Ahmad M, Hollender L, Anderson Q, Kartha K, Ohrbach R, Truelove EL, et al. Research diagnostic criteria for temporomandibular disorders (RDC/TMD): Development of image analysis criteria and examiner reliability for image analysis. *Oral Surgery, Oral Medicine, Oral Pathology, Oral Radiology and Endodontics*. 2009; 107:844–860.
9. Schiffman E, Ohrbach R, Truelove E, Look J, Anderson G, Goulet JP, et al. Diagnostic Criteria for Temporomandibular Disorders for Clinical and Research Applications: recommendations of the International RDC/TMD Consortium Network* and Orofacial Pain Special Interest Group. *J Oral Facial Pain Headache*. Winter. 2014; 28:6–27. [PubMed: 24482784]
10. Alexiou K, Stamatakis H, Tsiklakis K. Evaluation of the severity of temporomandibular joint osteoarthritic changes related to age using cone beam computed tomography. *Dento Maxillo Facial Radiology*. 2009; 38:141–147. [PubMed: 19225084]
11. Schilling J, Gomes LC, Benavides E, Nguyen T, Paniagua B, Styner M, et al. Regional 3D superimposition to assess temporomandibular joint condylar morphology. *Dentomaxillofac Radiol*. 2013; 43:20130273. [PubMed: 24170802]
12. Slicer.org. Surgical Planning Laboratory, Harvard Medical School; Boston: [homepage on the internet] [updated 2014 Sep 01]. Available: <http://download.slicer.org> [2014 Sep 01]

13. Itksnap.org. Penn Image Computing and Science Laboratory, University of Pennsylvania; Philadelphia: [homepage on the internet] [updated 2014 May 17]. Available: <http://www.itksnap.org> [2014 Sep 01]
14. Cevidanes LH, Hajati AK, Paniagua B, Lim PF, Walker DG, Palconet G, et al. Quantification of condylar resorption in temporomandibular joint osteoarthritis. *Oral Surg Oral Med Oral Pathol Oral Radiol Endod.* 2010; 110:110–7. [PubMed: 20382043]
15. Paniagua B, Cevidanes LHS, Walker D, Zhu H, Guo R, Styner M. Clinical application of SPHARM-PDM to quantify temporomandibular joint osteoarthritis. *Computerized Medical Imaging and Graphics.* 2011; 35:345–52. [PubMed: 21185694]
16. Styner M, Oguz I, Xu S, Brechbühler C, Pantazis D, Levitt JJ, et al. Framework for the Statistical Shape Analysis of Brain Structures using SPHARM-PDM. *Insight J.* 2006; 1071:242–250. [PubMed: 21941375]
17. Spharm-PDM. Neuro Image Research and Analysis Laboratories, University of North Carolina; Chapel Hill: [homepage on the Internet]. [updated 2014 Jul 21]. Available: <http://www.nitrc.org/projects/spharm-pdm> [2014 Sep 01]
18. Shape Analysis Mancova [homepage on the Internet]. Neuro Image Research and Analysis Laboratories, University of North Carolina; Chapel Hill: [updated 2014 June 27]. Available: http://www.nitrc.org/projects/shape_mancova [2014 Sep 01]
19. Paniagua, B.; Styner, M.; Macenko, M.; Pantazis, D.; Niethammer, M. [2014 Sep 15] Local shape analysis using MANCOVA.. *Insight Journal* [serial on the Internet]. Sep. 2009 [about 21 p.]. Available: <http://www.insight-journal.org/browse/publication/694>
20. Qiao X, Zhang HH, Liu Y, Todd MJ, Marron JS. Weighted Distance Weighted Discrimination and its Asymptotic Properties. *Journal of the American Statistical Association.* 2009; 105:401–414. [PubMed: 21152360]
21. Stratemann SA, Huang JC, Maki K, Hatcher DC, Miller AJ. Evaluating the mandible with cone-beam computed tomography. *Am J Orthod Dentofacial Orthop.* 2010; 137:S58–S70. [PubMed: 20381763]
22. Williams FM. Biomarkers: In combination they may do better. *Arthritis Research & Therapy.* 2009; 11:130. [PubMed: 19886980]
23. Samuels J, Krasnokutsky S, Abramson SB. Osteoarthritis: A tale of three tissues. *Bulletin of the NYU Hospital for Joint Diseases.* 2008; 66:244–250. [PubMed: 18937640]
24. Abramson SB, Attur M. Developments in the scientific understanding of osteoarthritis. *Arthritis Res Ther.* 2009; 11:227. [PubMed: 19519925]
25. Schneider E, Lo GH, Sloane G, Fanella L, Hunter DJ, Eaton CB, et al. Magnetic resonance imaging evaluation of weight-bearing subchondral trabecular bone in the knee. *Skeletal Radiol.* 2011; 40:95–103. [PubMed: 20449585]
26. Johnston JD, McLennan CE, Hunter DJ, Wilson DR. In vivo precision of a depth-specific topographic mapping technique in the CT analysis of osteoarthritic and normal proximal tibial subchondral bone density. *Skeletal Radiol.* 2011; 40:1057–64. [PubMed: 20814786]
27. Langs G, Peloschek P, Bischof H, Kainberger F. Automatic quantification of joint space narrowing and erosions in rheumatoid arthritis. *IEEE Trans Med Imaging.* 2009; 28:151–64. [PubMed: 19116197]
28. Radin EL, Rose RM. Role of subchondral bone in the initiation and progression of cartilage damage. *Clin Orthop Relat Res.* 1986; 213:34–40. [PubMed: 3780104]

Clinical Relevance

This study investigated morphological variations in 169 Temporomandibular Joint (TMJ) condyles, using novel imaging modeling approaches. Direction-Projection-Permutation statistics supported significant differences between the healthy control and TMJ osteoarthritis (OA) groups, even at initial diagnosis, with targeted classification of the severity and location of morphological differences. The TMJ condylar bone is the site of numerous dynamic morphological transformations, which are an integral part of the initiation/progression of OA, not merely secondary manifestations to cartilage degradation.

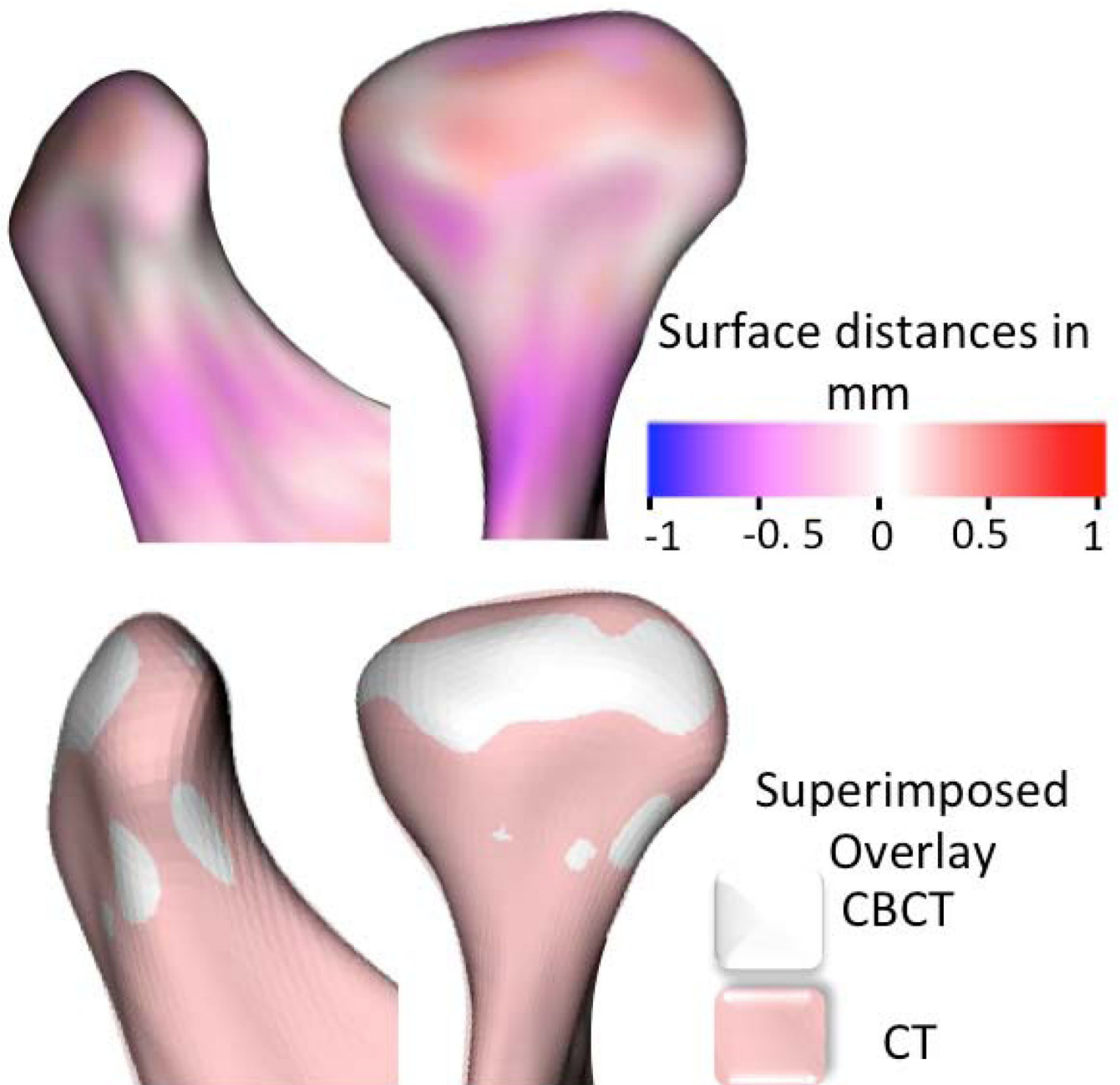


Figure 1.

The use of CBCT images to detect bony changes requires an adequate image acquisition protocol and precise construction of surface models. This figure compares the 3D surface models constructed from CT (shown in pink) and CBCT (shown in white) images of the same subject using correspondent distances in the top row and semitransparent overlays in the bottom row. Differences between the CBCT and CT models are smaller than 0.5 mm.

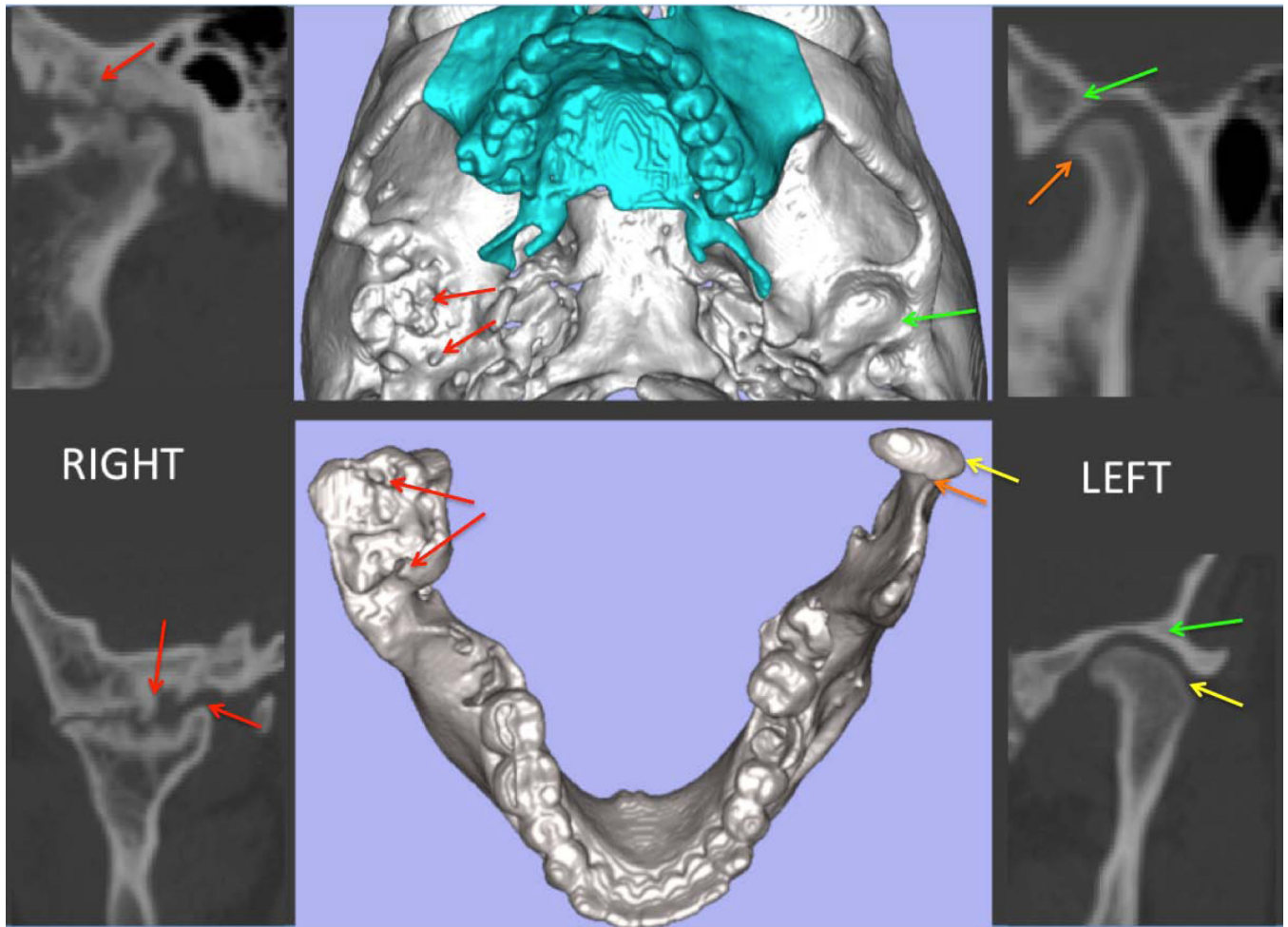


Figure 2. CBCT cross-sections and 3D models for a patient with ankylosis on the right side and OA on the left side; these are examples of exclusion and inclusion criteria, respectively. Note that red arrows indicate bony proliferations on the condyle and subchondral lesions in the articular fossa on the ankylosed right side. These findings differ from the left side that presents with osteoarthritic changes exemplified by flattening of the lateral pole (yellow arrows) and a bony projection on the anterior condylar surface (orange arrows), without dysmorphology of the articular fossa (green arrows).

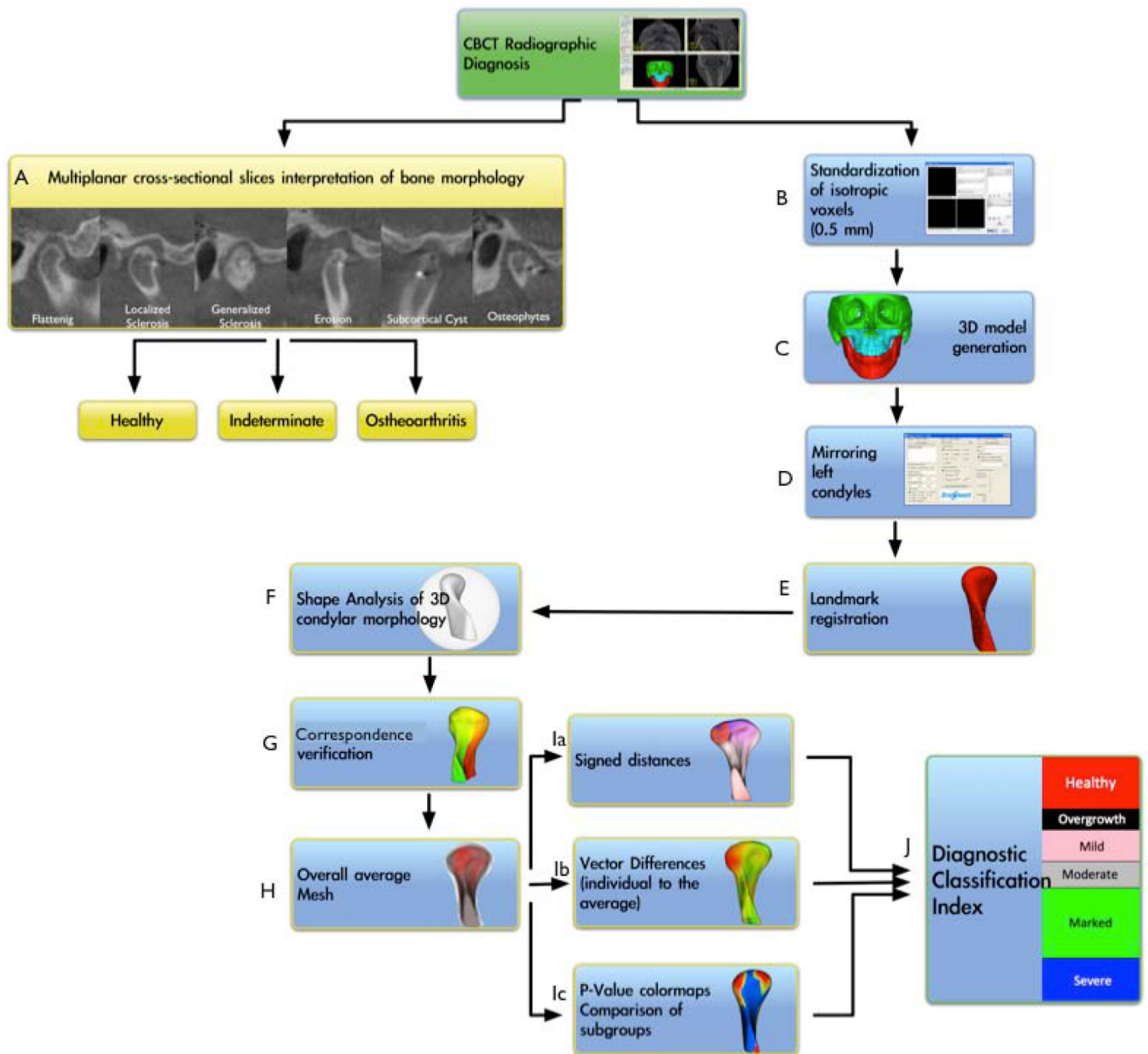


Figure 3. Flowchart of the image analysis procedures. A. Radiographic diagnoses of TMJ health or disease in multiplanar cross-sections; B. Standardization of voxel size; C. Construction of surface models; D. Mirroring of left condyles to form right condyles; E. Landmark registration; F. SPHARM-PDM spherical parameterization of 1002 correspondent mesh point-based models; G. Correspondence verification; H. Construction of average healthy, initial diagnosis, and long-term history of OA surface meshes; Ia. Computation of surface distances between groups; Ib. Computation of vector differences; Ic. P-value color-coded maps showing the surfaced with statistically significant condylar morphological differences; J. Diagnostic classification of the severity of condylar morphological changes

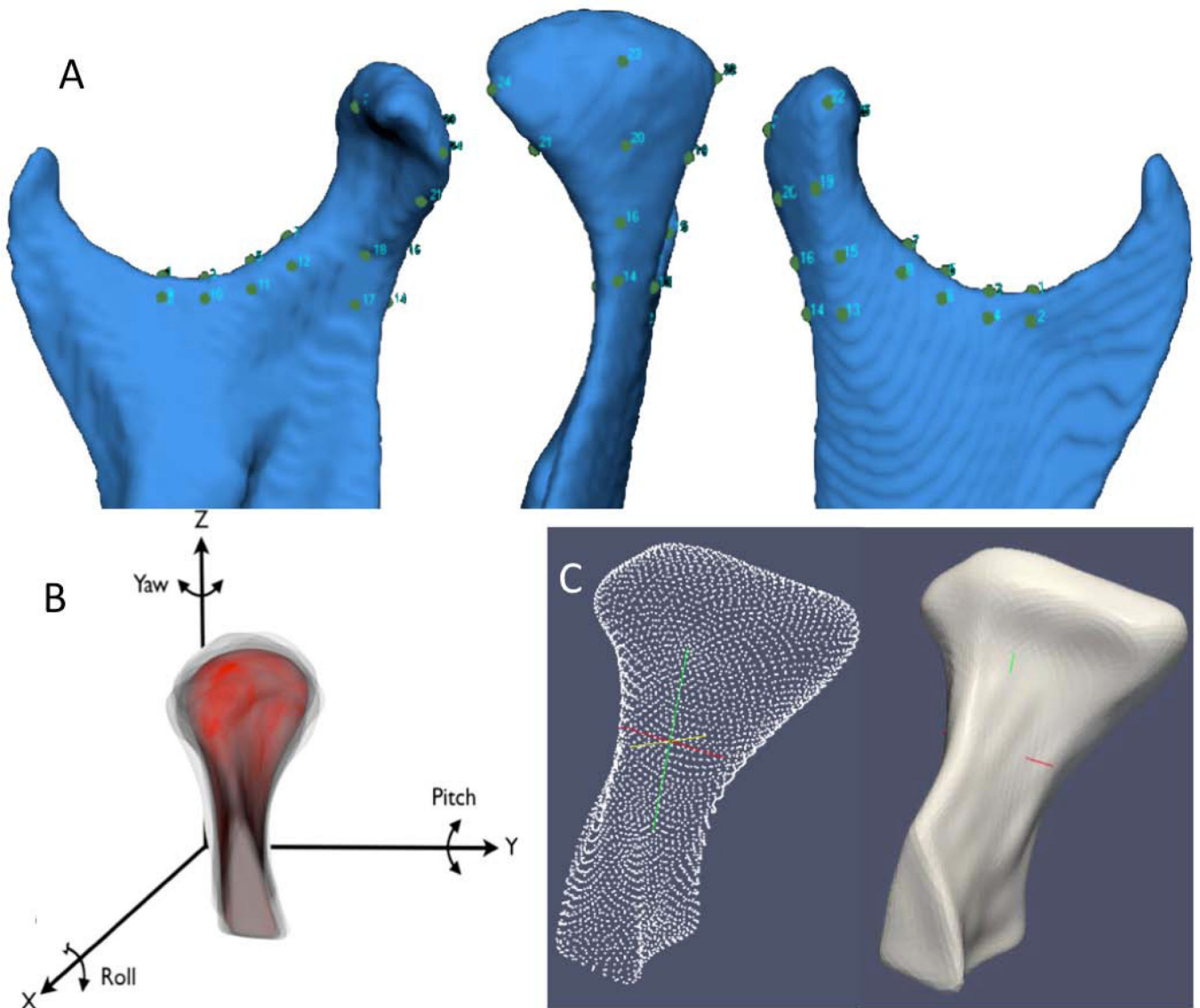
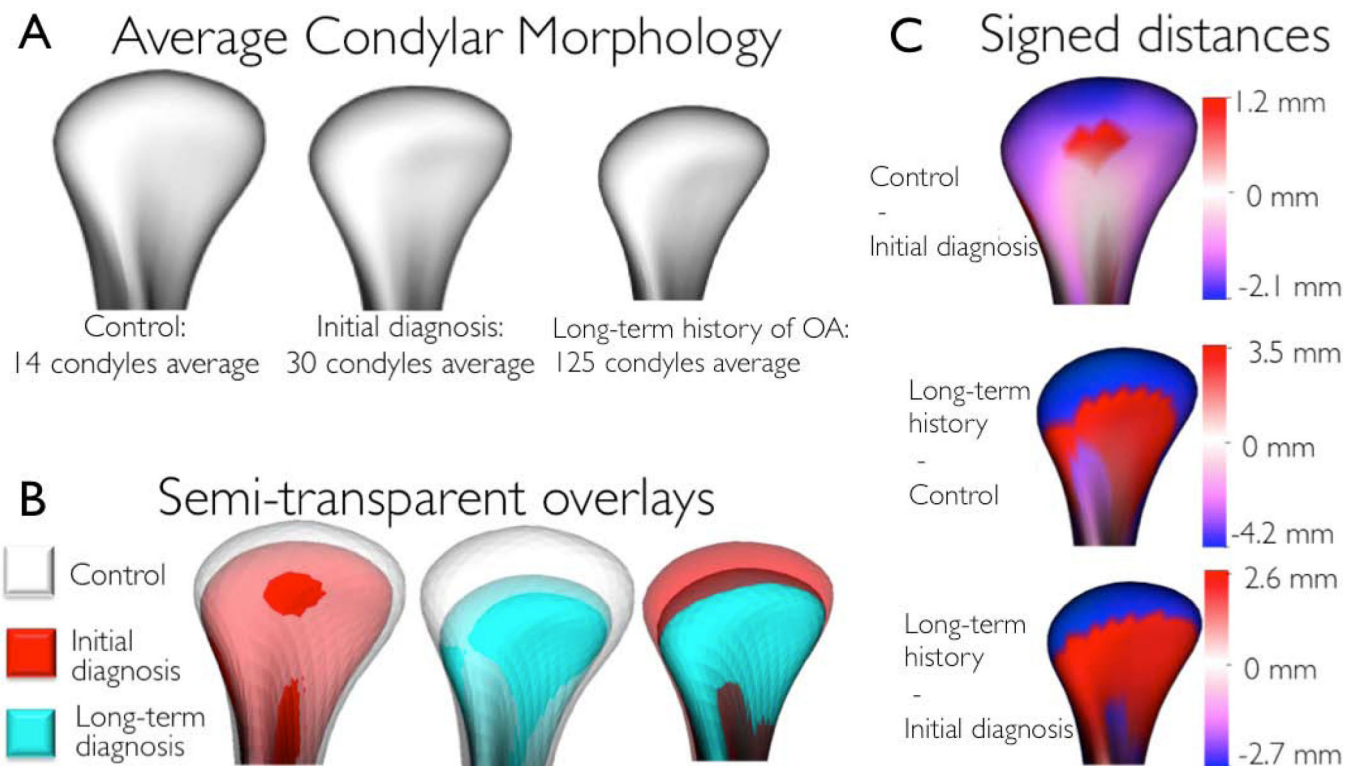


Figure 4.

A and B. Landmark-based registration used to approximate condyles from all subjects in the group comparisons. A. 25 points in the ramus and condyle surfaces used for the landmark-based registration; B. Reference condylar model (red) with the overlays of multiple condyles approximated in the same co-ordinate system. Note that the xyz coordinate system is common to all models after registration and uses as reference an arbitrary condyle in the sample to standardize the co-ordinate system across all condyles; C. Parameterization of 1,002 homologous or correspondent surface mesh points for statistical comparisons and detailed phenotypic characterization of the surface models.

**Figure 5.**

A. Average condylar morphologies; B. Semi-transparent overlays of group average morphologies; C. Quantitative assessment of condylar morphology is shown in signed distance color-coded maps computed locally at each correspondent surface point: blue areas (– values) are indicative of bone resorption and red areas (+ values) are indicative of bone overgrowth.

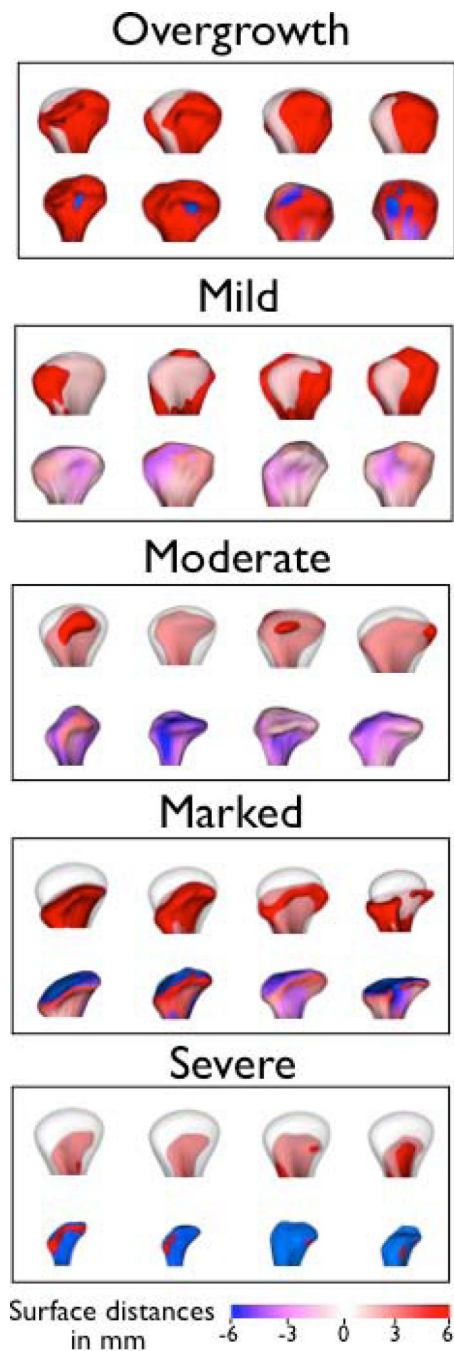


Figure 6.

Examples of condyles in each preliminary subgroup established by comparison of each individual condyle and the healthy controls' average morphology. The top row in each box shows semitransparency overlays of each condyle (red) and the average control condyle (transparent white). The bottom row in each box shows the subtraction between each condyle and the average control condyle with differences displayed with signed distances, where red describes areas indicative of bone proliferation and blue areas of bone resorption. The overgrowth group presented morphological deformations with marked bone

proliferation. The predominantly resorptive/degenerative groups were categorized as mild, moderate, marked or severe resorption.

Author Manuscript

Author Manuscript

Author Manuscript

Author Manuscript

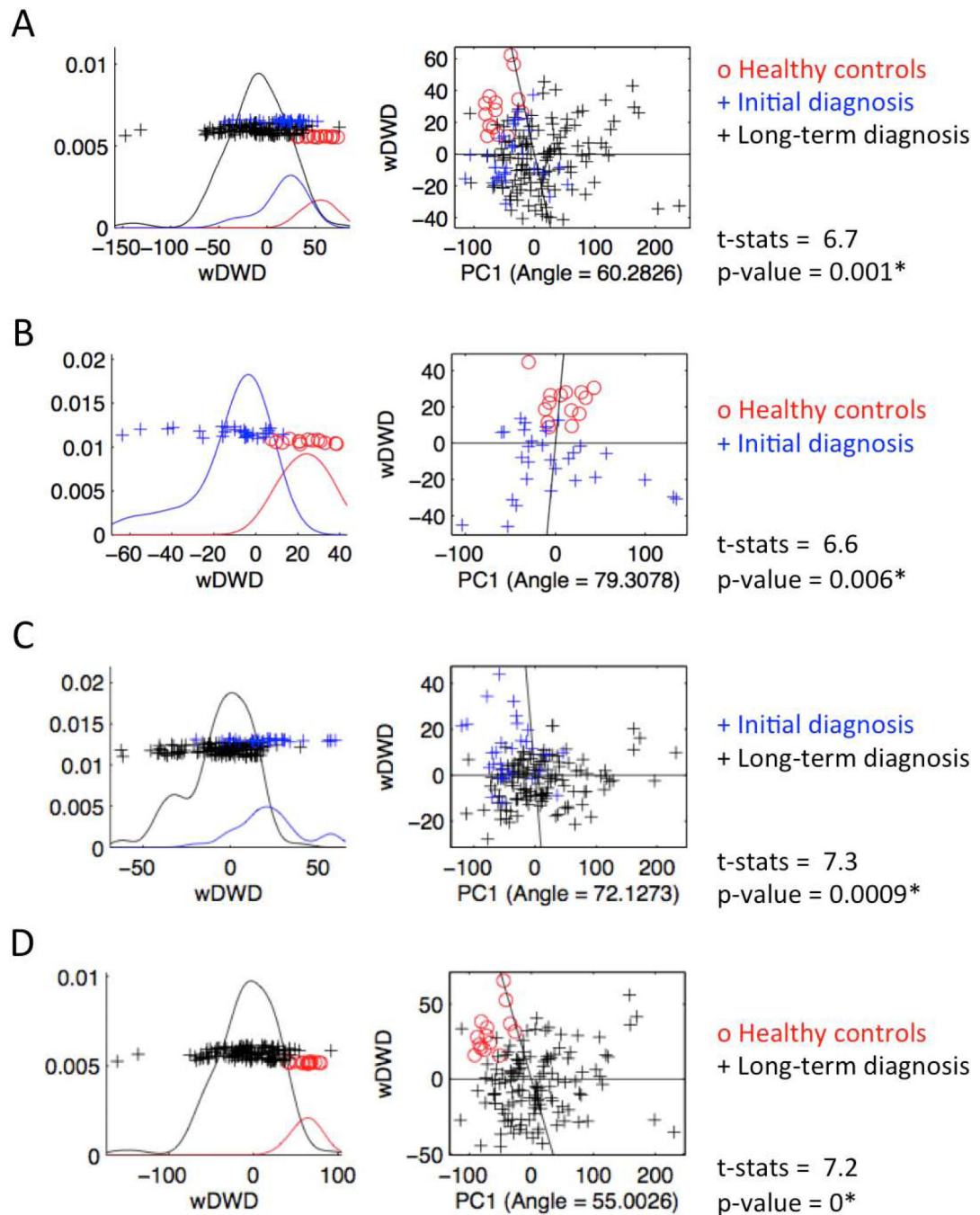


Figure 7.

DiProPerm graphic results. The left panels show the distribution of the data projected onto the DWD direction, illustrating how well the groups listed in the right panels can be separated. The curves in the left panel are smooth histograms, with each color showing the sub-histograms for that group. The center panel shows principal component graphics, where each condyle is plotted in the first principal direction. The horizontal x-axis is the projected value, and the vertical y-axis reflects order in the data set, to avoid overplotting.

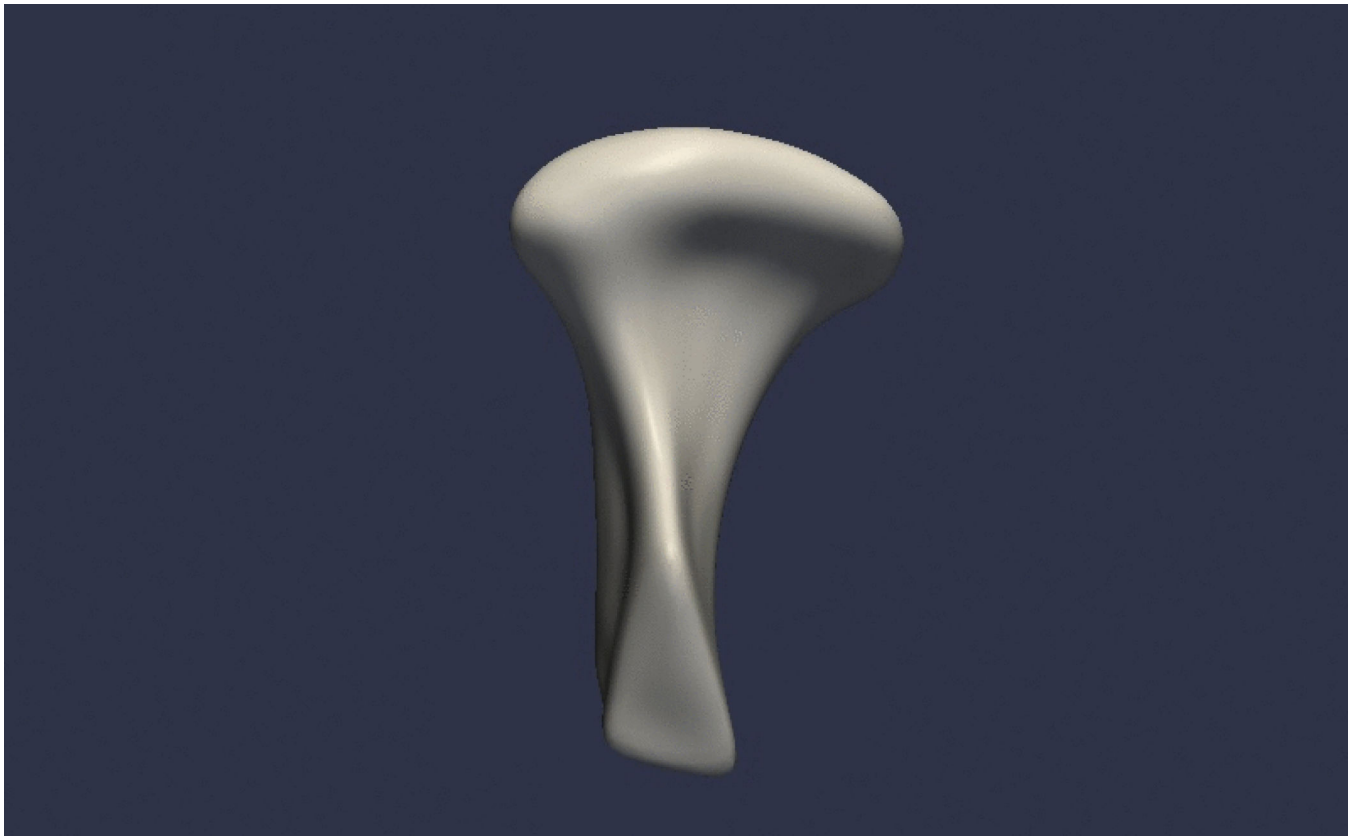


Figure 8.
Graphic display of the first principal component of morphological variability.